

See discussions, stats, and author profiles for this publication at: <https://www.researchgate.net/publication/222735381>

Doppler-based detection and tracking of humans in indoor environments

Article in *Journal of the Franklin Institute* · September 2008

DOI: 10.1016/j.jfranklin.2008.04.001

CITATIONS

97

READS

416

4 authors:



Shobha Sundar Ram

Indraprastha Institute of Information Technology

60 PUBLICATIONS 814 CITATIONS

[SEE PROFILE](#)



Yang Li

Shanghai Institute of Materia Medica, Chinese Academy of Sciences, China, Shang...

63 PUBLICATIONS 640 CITATIONS

[SEE PROFILE](#)



Adrian Lin

University of Texas at Austin

13 PUBLICATIONS 408 CITATIONS

[SEE PROFILE](#)



Hao Ling

University of Texas at Austin

386 PUBLICATIONS 9,536 CITATIONS

[SEE PROFILE](#)

Some of the authors of this publication are also working on these related projects:



Antenna mutual coupling and platform effects [View project](#)



Human tracking and imaging [View project](#)



Doppler-based detection and tracking of humans in indoor environments

Shobha Sundar Ram^{*}, Yang Li, Adrian Lin, Hao Ling

Department of Electrical and Computer Engineering, The University of Texas at Austin, 1 University Station, Austin TX 78712-1084, USA

Received 19 September 2007; received in revised form 2 April 2008; accepted 9 April 2008

Abstract

In this paper, the principles of Doppler processing to detect and track human movers in indoor environments are presented. The topics discussed include the micro-Doppler characteristics of humans, the azimuth, elevation and range tracking of humans using Doppler, spatial and frequency diversity, the effect of walls, and the characteristics of dynamic clutters from non-humans. The studies are supported by simulation and measurement results.

© 2008 The Franklin Institute. Published by Elsevier Ltd. All rights reserved.

Keywords: Doppler radar; Spectrogram; Micro-Doppler; Direction of arrival; Human tracking; Through-wall radar

1. Introduction

Through-wall radar imaging is a topic of current research interest in connection with law enforcement, urban area operations and search and rescue missions. Developments to date include wideband radar using impulsive [1–4] or stepped frequency [5,6] waveforms to obtain down-range resolution down to a few centimeters. Since the attenuation of the signal through walls increases rapidly as a function of frequency [7,8], frequencies below 5 GHz are usually employed. One particular aspect of through-wall imaging is the monitoring of human activities. For human movement detection and tracking, Doppler

^{*}Corresponding author. Tel./fax: +1 512 471 1910.

E-mail addresses: shobhasram@mail.utexas.edu (S.S. Ram), yangl@mail.utexas.edu (Y. Li), adrian.lin@innowaveresearch.com (A. Lin), ling@ece.utexas.edu (H. Ling).

sensing is a natural choice since stationary indoor clutters can be suppressed to highlight human movements. Further, low-cost, low-power Doppler sensors can be readily implemented. Finally, human movements give rise to very unique micro-Doppler features [9–11], which may be exploited for recognition [12,13]. An early example of a Doppler-based system is the motion detector radar with a continuous wave phase detector to detect moving targets [14]. However, this system does not provide any location information. The Radar Flashlight system that was later developed in [15,16] utilizes an X-band FMCW radar system to detect the respiratory motion of still humans behind walls. In [17], a pulse-Doppler waveform is used to compute the range of humans through walls. By using a real array with multiple elements, the bearing information in azimuth and elevation could also in principle be obtained, although at the expense of higher cost. Use of synthetic aperture concept is more challenging due to the short time required to collect coherent data from the human movement.

In this paper, we discuss the application of the Doppler concept to detect and track humans in complex indoor environments. First, we focus on the micro-Doppler characteristics of humans. In Section 2, human gait data are represented in the joint time–frequency space using the short-time Fourier transform (STFT). The Doppler spectrograms of both simulated and measured data are studied to identify various movements. The reassigned joint time–frequency transform (RJTF) [18–21] is also explored for its superior signal localization properties to aid the interpretation of the micro-Doppler features.

Next, we focus on the use of Doppler sensors to track multiple human subjects indoors. A low-complexity Doppler radar concept [22–27] is first reviewed in Section 3. The concept exploits the Doppler separation among movers to track multiple humans in three dimensions using only three antenna elements and two carrier frequencies. In Section 4, we study ways to improve the multiple-human tracking performance. We show that by incorporating a multiple element array, it is possible to combine Doppler processing with spatial beamforming to resolve different targets in the Doppler and bearing space [28]. Additional frequency diversity is also explored to determine the range of targets.

Finally, some of the challenges to Doppler-based human tracking are discussed. In Section 5, we study the effect of walls on the signal amplitude decay and phase distortion. These wall effects can cause significant degradation in the signal-to-noise ratio as well as error in the bearing estimation of humans through walls. This is studied using both simulations based on the finite-difference time-domain (FDTD) simulation as well as measurements on real walls. Conclusions are given in Section 6.

2. Micro-Doppler characteristics of human movements

Contrary to rigid targets commonly encountered in many radar applications, a human is a complex non-rigid body under movement. As a result, many interesting features of human movement such as the swinging arms and legs can be observed using a Doppler radar. These features are termed micro-Dopplers and they have been studied in a number of publications [9–11,29,30] through the use of joint time–frequency representations.

We first illustrate the micro-Dopplers from human gait using simulation data. The methodology is similar to that reported in [11], which uses a primitive-based model to simulate the radar returns from different parts of the human body. The human body is modeled as a complex target with 12 body parts as shown in Fig. 1a. The head is modeled

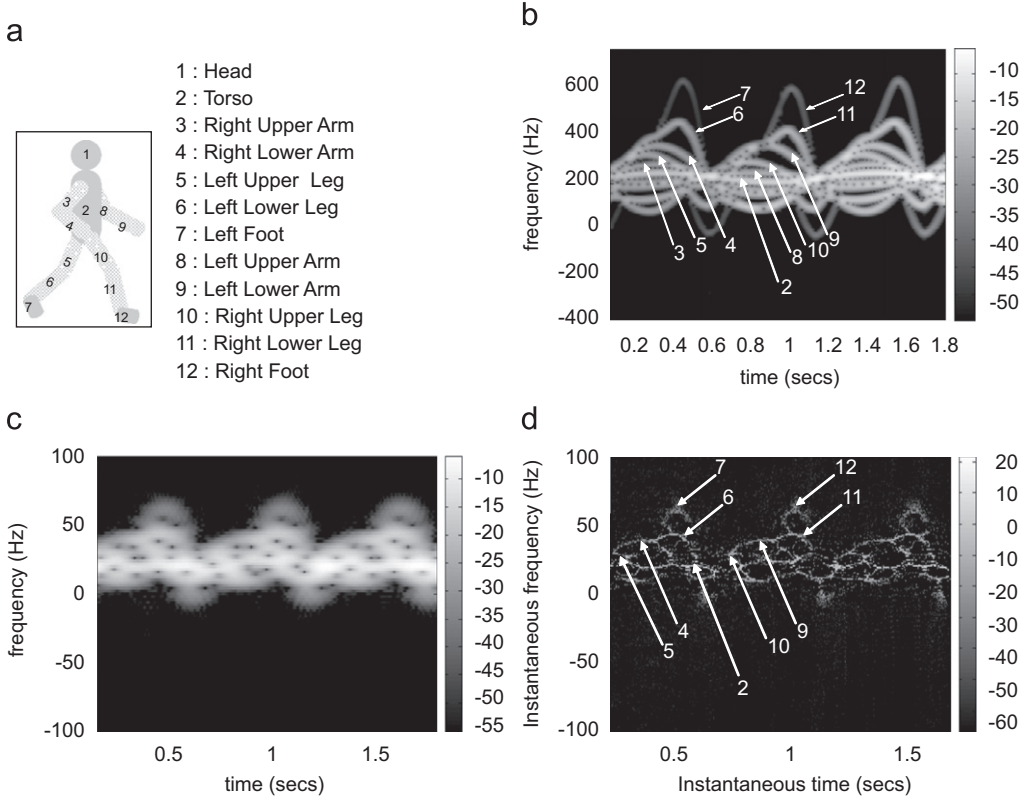


Fig. 1. (a) Simulation model of human walking at 1.4 m/s towards a Doppler radar. STFT of simulated returns for a carrier frequency of: (b) 24 GHz, (c) 2.4 GHz. (d) Reassigned JTF of simulated returns for a carrier frequency of 2.4 GHz.

as a perfectly conducting sphere and the other body parts are modeled as perfectly conducting ellipsoids of standard dimensions. As the center of gravity (CG) of the human moves, the position of each body part is specified with respect to the CG using time-varying functions described by the Thalmann model [31]. The time-varying radar cross section (RCS) of the human target is then obtained by the complex sum of the RCS of the individual body parts. This is then used in the radar range equation to generate the radar return signal as a function of time. The Doppler spectrogram, $|\chi|^2$, is generated by the application of the STFT on the time domain radar data, $x(t)$, as

$$\chi(t, f) = \int x(t') e^{-(t-t')^2/2\sigma^2} e^{+j2\pi f(t-t')} dt' = |\chi| e^{j\phi} \tag{1}$$

Here, a Gaussian window with a time width of σ is used in the STFT.

Fig. 1b shows the Doppler spectrogram that is generated when a carrier frequency of 24 GHz is used in the simulation. The human subject is assumed to approach the radar head-on at a velocity of 1.4 m/s along a straight line path. A time window width σ of 0.25 s is used throughout the paper. We observe that distinct time-varying Doppler tracks due to the motions of each of the parts of the body (labeled as 2–12) are resolved in the

spectrogram. The strongest returns are from the torso (2) and the highest Doppler frequency arises from the motion of the lower legs (6, 11) and feet (7, 12). It is clearly seen that the motion of the right arm (3, 4) accompanies the motion of the left leg and foot (5, 6, 7) and vice versa. The superior Doppler sensitivity results from the high carrier frequency chosen for the simulation. However, signal attenuation through walls at such a high frequency is very severe and a much lower frequency is needed for wall penetration. Fig. 1c shows the Doppler spectrogram that is generated when a carrier frequency of 2.4 GHz is used in the simulation. It is now difficult to discern the various micro-Doppler components in the spectrogram. Hence there is a tradeoff between Doppler sensitivity and signal penetration through walls.

One interesting question is whether the Doppler sensitivity problem at a low operating frequency can be overcome through the use of joint time–frequency representations other than the STFT. Here we investigate a potential candidate called the reassigned joint time–frequency (RJTF) transform. The reassigned spectrogram was first developed by Kodera et al. [18] in 1978, and later adopted by the acoustics community [19–21]. The basic idea of the method is to transform $|\chi|^2$ from the time–frequency (t – f) domain to the instantaneous time versus instantaneous frequency (t_{ins} – f_{ins}) domain. The t_{ins} and f_{ins} coordinates are derived from the partial derivatives of the phase of the STFT spectrogram, φ , as

$$f_{\text{ins}} = \frac{1}{2\pi} \frac{\partial \varphi}{\partial t} \quad (2)$$

$$t_{\text{ins}} = t - \frac{1}{2\pi} \frac{\partial \varphi}{\partial f} \quad (3)$$

In our implementation, the phase derivatives are derived using the formulas discussed in [21]. Each point in the STFT spectrogram is then reassigned to the coordinate positions (t_{ins} , f_{ins}) and appropriately weighted to ensure that energy is conserved during the transformation. This results in the reassigned distribution in the t_{ins} – f_{ins} plane. The computational complexity of RJTF algorithm is twice that of the STFT operation. The main characteristic of the reassigned distribution is that the signal energy is localized to thin lines of high precision. This contrasts with the STFT distribution where the thickness of each signal feature is defined by σ along the time axis and $1/\sigma$ along the frequency axis. Fig. 1d shows the reassigned spectrogram of the same data as those processed in Fig. 1c. It is now possible to discern up to nine distinct micro-Doppler tracks (2, 4, 5, 6, 7, 9, 10, 11 and 12). Since the signal energy has been focused in the RJTF, the dynamic range of the reassigned spectrogram differs from that of the STFT spectrogram. It is also important to point out that while RJTF leads to improved readability compared to the STFT spectrogram, the resolution of the reassigned transform is still limited by the Fourier uncertainty bounds. That is, it is possible to perfectly resolve two features only if they are farther apart than σ along the time axis and $1/\sigma$ along the frequency axis.

The unique characteristics of the micro-Doppler features make the human Doppler spectrograms potentially useful for identifying and classifying different types of movements [12,13]. This is illustrated by examining the spectrograms of some deviated walking motion data collected using a Doppler radar testbed. The radar testbed consists of a transmitter with an RF signal generator at 2.4 GHz and a horn antenna. The receiver consists of a microstrip antenna and an integrated quadrature receiver (AD8347) where the

signal is amplified and downconverted. A 12 bit, 1000 Hz A/D converter (NI-DAC 6024E) is used to digitize the time-domain receiver output. In the first measurement, the human subject walks toward the radar head-on from a distance of 10 m (Fig. 2a). The RJTF transform is applied to the radar data and the resulting reassigned spectrogram is shown in Fig. 2b. It is observed that the Doppler track of the torso (2) is first positive, then negative during the 7 s data collection. Some of the micro-Doppler features can be identified in the spectrogram such as the feet (7, 12), lower legs (6, 11) and lower arms (4, 9). Due to the periodic nature of the human walking motion, the micro-Doppler's features of the different body parts are observed for every stride of the human motion.

Next the subject repeats the same motions while carrying a metal corner reflector in his right hand (Fig. 2c). The reassigned Doppler spectrogram of the data is generated and presented in Fig. 2d. It is observed that the Doppler spectrogram in Fig. 2d is almost

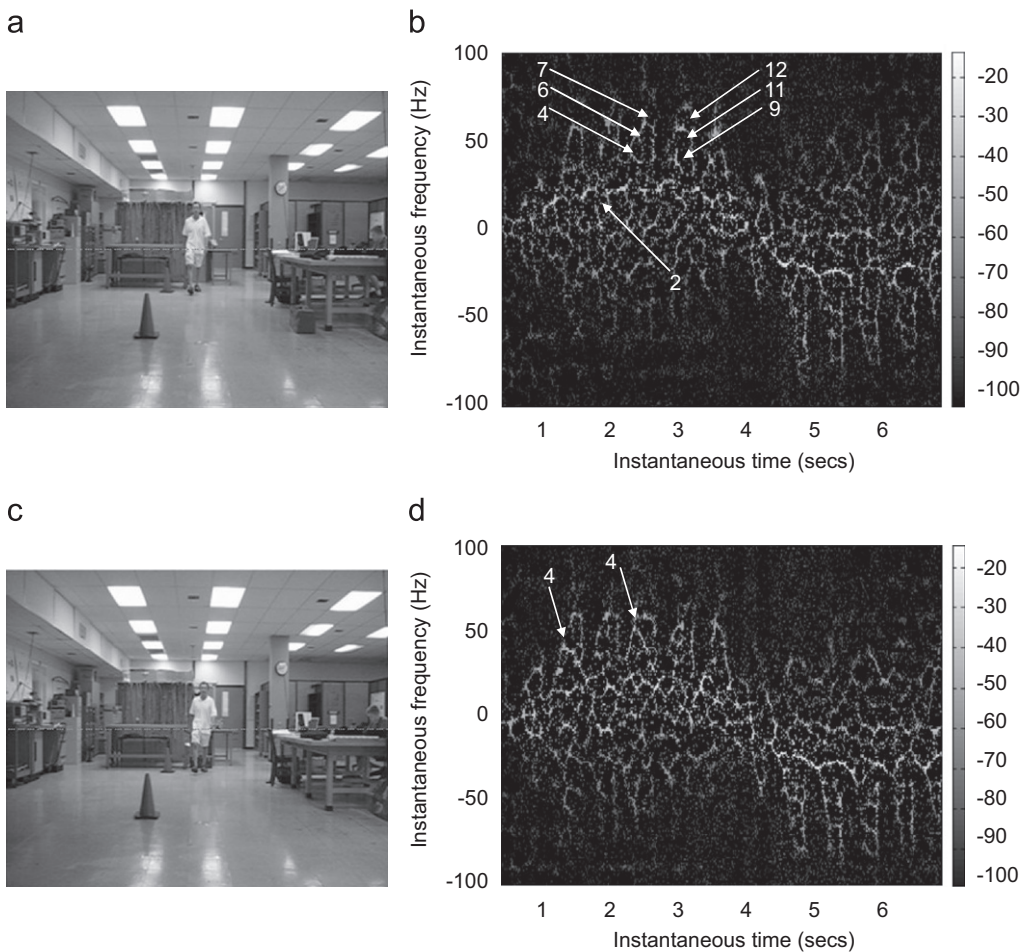


Fig. 2. (a) Case 1: walking human subject, (b) reassigned spectrogram of case 1. (c) Case 2: walking human subject holding a light horn reflector in the right hand, (d) reassigned spectrogram of case 2. (e) Case 3: walking human subject holding a heavy metal box on his right with both hands, (f) reassigned spectrogram of case 3. (g) Case 4: walking human subject holding a pole in the right hand, (h) reassigned spectrogram of case 4.

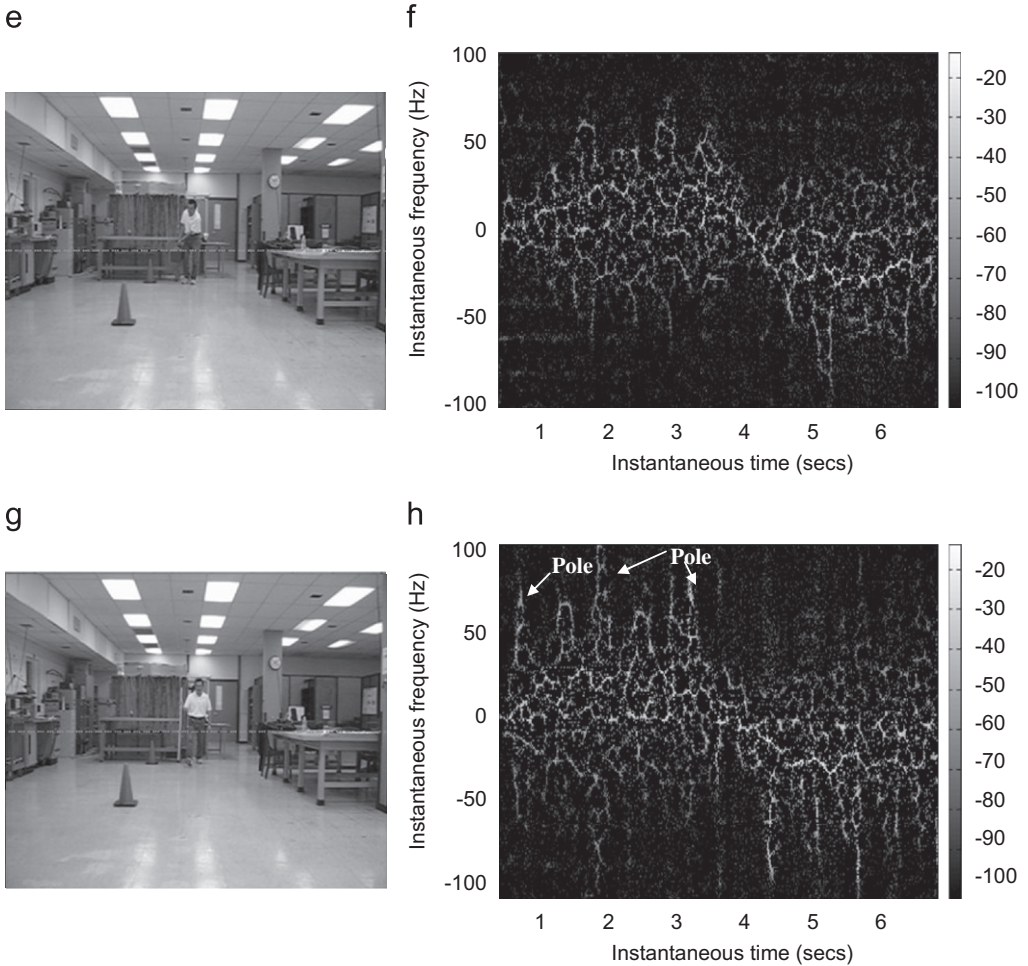


Fig. 2. (Continued)

identical to that in Fig. 2b, except that the micro-Doppler feature from the right hand (4) has been enhanced. In the next measurement, the subject walks the same path while carrying a heavy box using both hands as shown in Fig. 2e. This action causes the subject's walking pattern to change considerably and is reflected in the reassigned spectrogram shown in Fig. 2f. The Doppler features of the right leg and foot are altered since that leg moves slower than the other one. The Dopplers of both arms are also changed, though more subtly. In the last measurement, the subject repeats the same path while using a long metal pole in his right hand, like a walking stick, as shown in Fig. 2g. In the reassigned spectrogram of the motion shown in Fig. 2h, a high Doppler component is observed slightly ahead of the Dopplers due to the right leg, caused by the motion of the pole. It is clear from these measurements that different walking patterns give rise to noticeable variations in the Doppler spectrogram features. Such variations may offer opportunities for classifying the different motion patterns in human movements.

3. Doppler-based human tracking

While the individual human Doppler was shown to be quite interesting, it is also desirable to simultaneously gather location information on multiple humans indoors. For this purpose, a very low-complexity radar concept that exploits the Doppler separation between multiple movers was investigated at the University of Texas [22–27]. The concept combines the Doppler discrimination offered by human movements with the direction of arrival (DOA) information that can be collected using a small antenna array to provide the necessary information for human movement tracking. For instance, provided multiple targets are moving at different radial velocities with respect to the radar, it is possible to determine the azimuth DOA or bearing of the targets using just two antenna elements spaced in the horizontal direction. The radar configuration is shown Fig. 3a. More explicitly, if we assume the time signals received at the two antenna elements to be $x_1(t)$ and $x_2(t)$, then after the Doppler processing the signals become $X_1(f)$ and $X_2(f)$, respectively. If the targets of interest generate different Doppler frequencies f_i due to the difference in their velocities with respect to the radar transceiver, then the DOA of target i with respect to the array boresight is given by

$$\theta_{AZi} = \sin^{-1} \left[\frac{\angle X_1(f_i) - \angle X_2(f_i)}{(2\pi d/\lambda_c)} \right] \quad (4)$$

where d is the spacing between the elements and λ_c is the RF wavelength. The hardware testbed constructed for this purpose is similar to that described in the previous section, except two receiver elements are employed. The element spacing d is chosen to be $\lambda_c/2$ to avoid angular aliasing. The STFT of the time domain radar signal is used to resolve the different targets along the Doppler domain and the DOA is determined using Eq. (4). Extensive data have been collected using this testbed and the results were reported in [23–25].

This concept has also been extended for two-dimensional azimuth-elevation tracking [26] and three-dimensional range-azimuth-elevation tracking [22]. The former is achieved through the use of a third antenna element directly above element 2 with a spacing of d as shown in Fig. 3b. The third element is connected to a separate receiver, Rx_3 , identical to the ones connected to elements 1 and 2. The elevation of a target, θ_{ELi} , with Doppler frequency f_i is computed from the phase difference of the Doppler-processed signals from channels 2 and 3 using

$$\Delta\phi_{23}(f_i) = \frac{2\pi d}{\lambda_c} \sin \theta_{ELi} \quad (5)$$

Ranging capability can also be achieved using the same concept by the incorporation of one additional frequency tone [27,32–35]. This is illustrated in Fig. 3c. Here two tones (2.39 and 2.4 GHz) are combined, amplified and transmitted simultaneously. An additional receiver channel, Rx_4 , with a local oscillator operating at 2.39 GHz is incorporated at the receiver system. The signal from antenna element 3 is split between Rx_3 and Rx_4 . The phase difference of the Doppler-processed signals received from Rx_3 and Rx_4 is used for computing the range R_i of the target at Doppler frequency f_i using

$$\Delta\phi_{34}(f_i) = \frac{4\pi\Delta f_c}{c} R_i \quad (6)$$

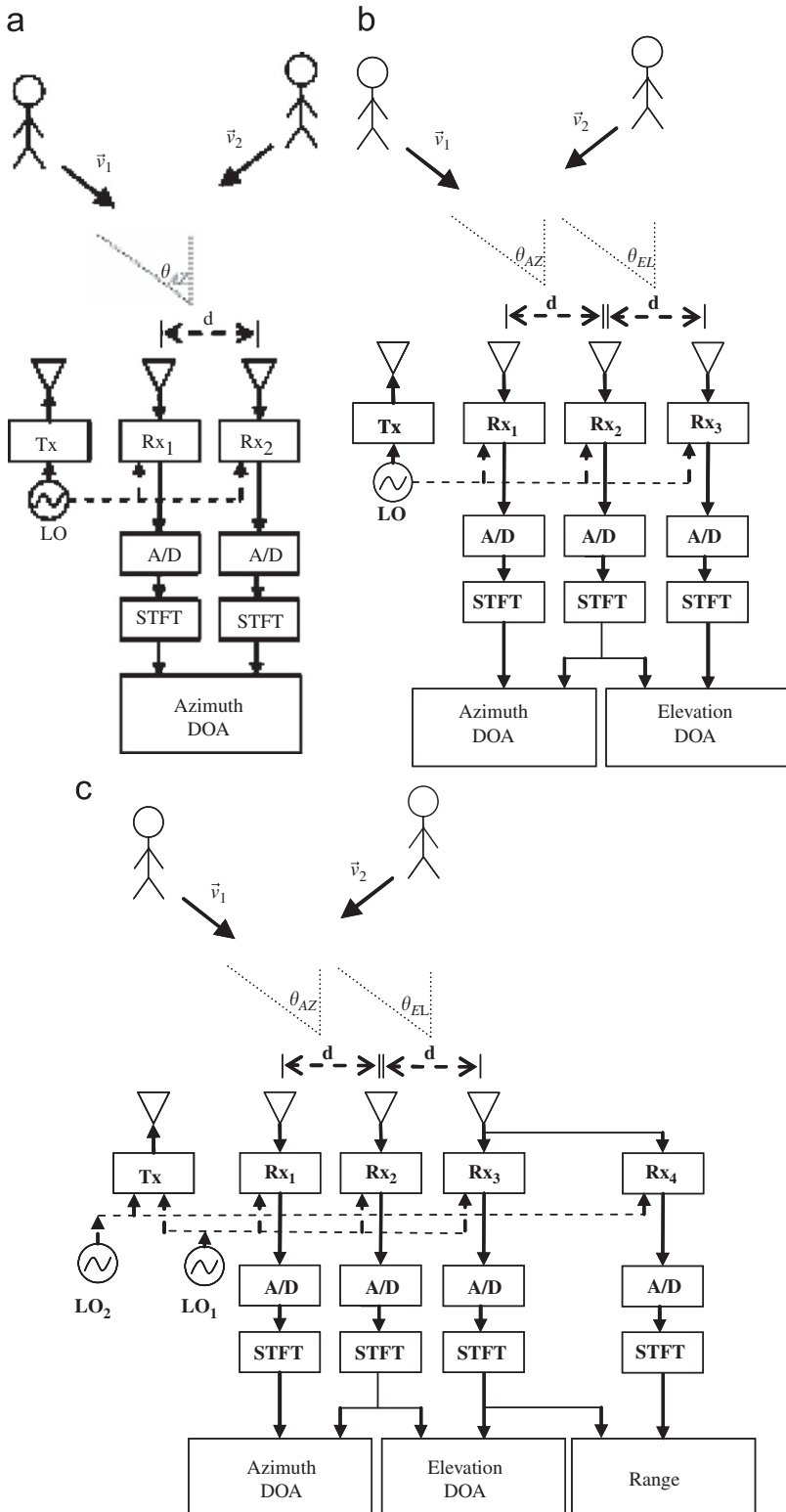


Fig. 3. (a) Two elements Doppler and direction-of-arrival radar. (b) Three elements two-dimensional Doppler and direction-of-arrival radar. (c) Three elements—two tones, three-dimensional radar.

Here Δf_c is the difference of the two tones (0.01 GHz) and is chosen to achieve a maximum unambiguous range of 15 m. Thus, by combining the two-dimensional bearing tracking with the ranging capability, full three-dimensional tracking can be achieved using only four receivers and three antenna elements in the resulting architecture.

Fig. 4 shows some representative results of tracking two human subjects through a 15 m exterior brick wall. Subject 1 approaches the radar from a distance of 13 m along a straight path and then turns and walks away from the radar. Subject 2 walks in a straight path in the opposite direction to subject 1 as shown in Fig. 4a. Hence the two subjects are well resolved in the Doppler domain as seen in the STFT spectrogram in Fig. 4b. The Doppler track of subject 1 is positive while the subject approaches the radar and negative when he moves away from the radar. The radar returns from the movers are processed to obtain the azimuth, elevation and the range estimation of the two subjects as a function of time. Fig. 4c shows the variation of the azimuth DOA of the two subjects with time. The azimuth of subject 1 varies from 0° to -30° while the azimuth of subject 2 varies from $+15^\circ$ to $+5^\circ$. The processed information in the range dimension is shown in Fig. 4d. As subject 1 initially approaches the radar, his range changes from 13 to 5 m. His subsequent range follows the away and then back pattern. The range of subject 2 follows the opposite pattern. Since both the subjects walk on the same ground level through out the time duration, the elevations of the two subjects remain approximately at 0° . This pattern is not shown in the figures. Finally, by using the range and azimuth information associated with each Doppler bin, it is possible to obtain a top *XY* view of the scene as a function of time. For display purposes, the time snapshots of the top view are summed in intensity to form a single plot in Fig. 4e. The tracks of the two subjects are clearly observed.

While the radar concept described in this section has very low complexity, it is based on the assumption that no two targets have the same Doppler returns. When the targets are not well resolved in the Doppler space, the errors in the DOA and range estimation are found to increase significantly. This problem is particularly acute for human tracking since micro-Doppler returns from human arm and leg motions have a broad Doppler spread. Therefore, the performance of the low-complexity concept is expected to degrade as the number of movers increase. Additional diversity must be incorporated to improve its performance. This will be discussed next.

4. Doppler tracking combined with spatial beamforming and frequency diversity

In this section, we study ways to improve the tracking performance of multiple humans with overlapping Dopplers. By combining Doppler processing with spatial beamforming in a multi-element (greater than 2) array, it becomes possible to resolve targets along two dimensions, Doppler and DOA. It is further possible to resolve targets along the range dimension by using multiple frequencies. The improvement in the performance towards multiple human tracking is first studied using Monte Carlo simulations. Next the algorithms for both two-dimensional Doppler–DOA tracking and three-dimensional Doppler–DOA–range tracking are tested using simulation data. Finally, measurements are conducted using a radar testbed to demonstrate two-dimensional Doppler–DOA tracking.

4.1. Monte Carlo simulation of multi-target tracking

Monte Carlo simulations are performed to investigate the performance improvement when additional diversities become available in space and frequency. The carrier frequency

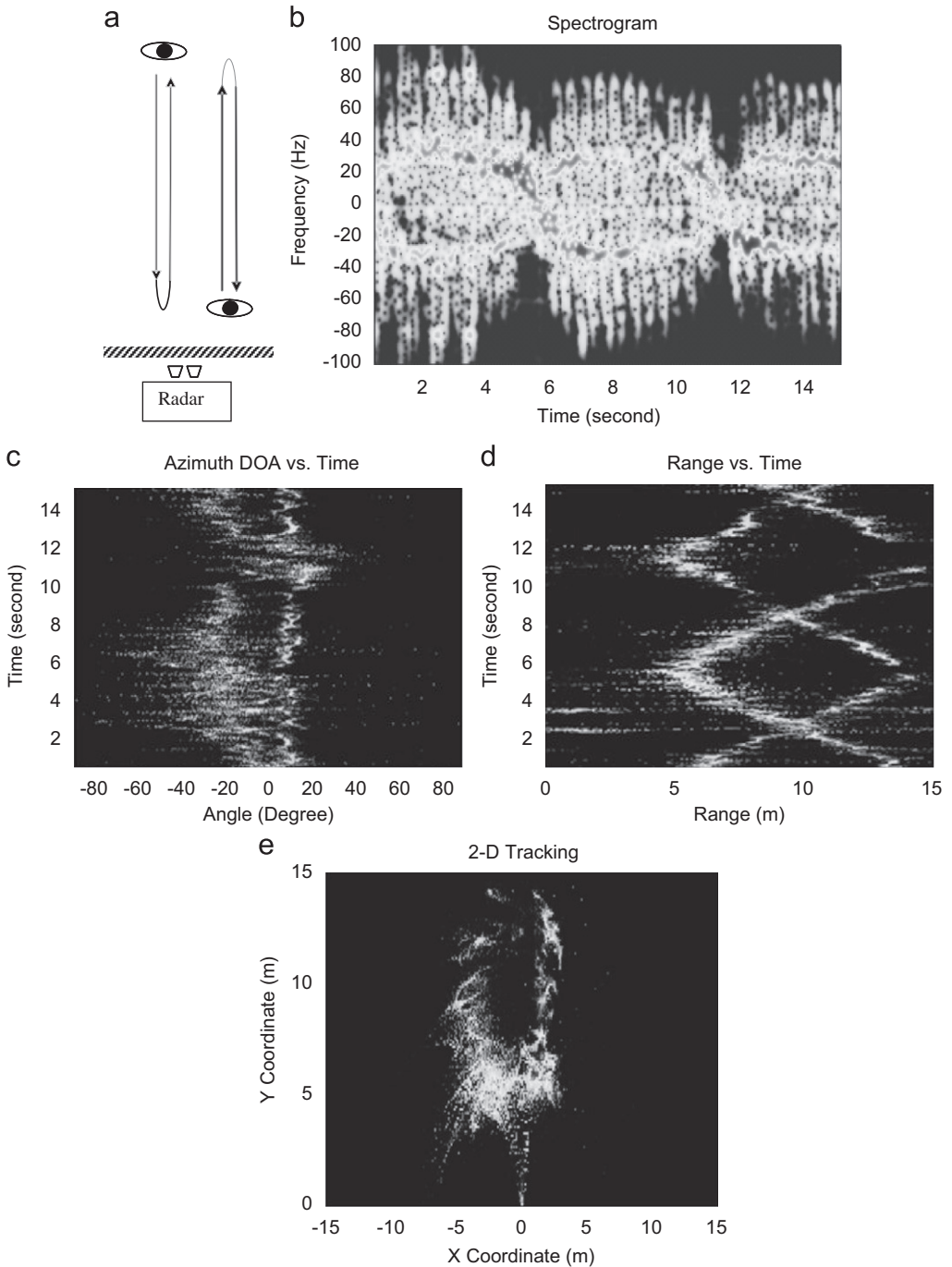


Fig. 4. (a) Illustration of multiple human subjects tracking through 15in brick wall (b) Doppler spectrogram of the two subjects. (c) Azimuth of the two subjects as a function of time. (d) Range of the two subjects as a function of time. (e) Top-view of the two subjects as a function of time.

of the system is assumed to be 2.4 GHz. For each realization of the Monte Carlo simulation, a given number of human subjects are randomly placed inside a region of space bounded in range from 1 to 30 m and DOA from -90° to $+90^\circ$. Each subject is randomly assigned a torso velocity with magnitude in the range of 0–2.5 m/s and direction in the range of 0° – 360° . The micro-Doppler spread of a single subject's return is on average around 20 Hz. Hence we assume that it is possible to resolve two targets in the 1-D Doppler dimension if their torso Dopplers are separated by more than 20 Hz. We next assume a 12-element array with an inter-element spacing of half wavelength. As a result, the 3 dB beamwidth is approximately 8° . By combining Doppler processing and spatial beamforming, each subject is resolvable in the 2-D Doppler–DOA space. We consider two subjects to be resolvable if their normalized Euclidean distance, $[(\text{Doppler}/20 \text{ Hz})^2 + (\text{DOA}/8^\circ)^2]^{1/2}$, is above 1. If we further assume that a stepped frequency waveform with a 120 MHz bandwidth and 5 MHz frequency step is used, then targets can be resolved up to a range resolution of 1.25 m with a maximum unambiguous range of 30 m. Again we consider two targets to be resolvable in the 3-D Doppler–DOA–range space if the normalized Euclidean distance between their 3-D centers is above 1. In general, a realization is regarded as successful if all the movers are resolvable. The simulation is performed for 100,000 realizations and the probability of successful resolution of multiple targets is computed and plotted in Fig. 5. It is observed that the probability of resolving targets based on Doppler discrimination alone (1-D) falls rapidly as the number of targets increases. The performance of the system is significantly improved by incorporating an additional DOA dimension (labeled as 2-D). When we incorporate the range dimension to form 3-D processing, there is again an improvement, although the increase is more moderate.

4.2. Combining Doppler processing with spatial beamforming

The procedure for combining Doppler processing with spatial beamforming for resolving multiple targets in the Doppler–DOA space is next discussed. First, we assume

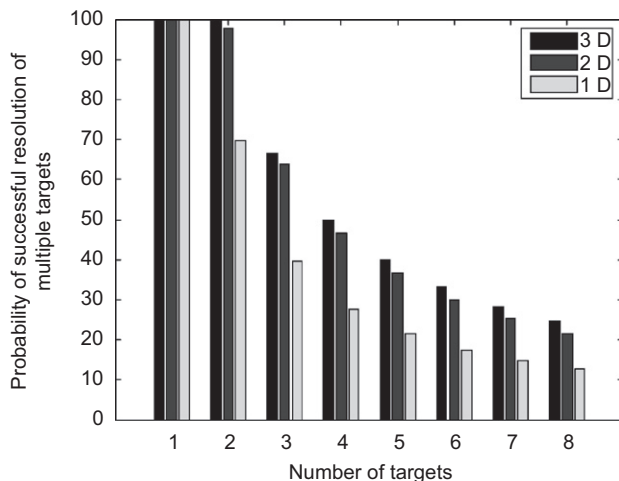


Fig. 5. Probability of successful resolution of multiple human radar returns for increased radar dimensions.

that a CW signal of carrier frequency, f_c , is transmitted. The scattered signals from moving humans are Doppler shifted and received by a radar system with an N element antenna array with inter-element spacing d . The radar returns are processed as

$$X(\sin \theta_{AZ}, f, t') = \sum_n \int_t x(n, t) e^{-j2\pi f t} h(t' - t) dt e^{-j(n-1)(2\pi f_c d/c) \sin \theta_{AZ}} \tag{7}$$

Here $x(n, t)$ is the time-domain received signal of element n of the array after the down conversion. The STFT of $x(n, t)$ is first carried out with time window, $h(t)$, to transform the signal from the time domain to the Doppler domain f . Then the signals are suitably phase shifted and summed to resolve the signal along the DOA (θ_{AZ}) dimension. As a result, for each time instant, t' , the radar returns are resolved along both the Doppler and DOA domains.

This technique is tested on simulated radar returns of moving humans obtained using the simulation model discussed in Section 2 and the radar parameters in Section 4.1. A number of different cases are tested. In case 1, we consider two human subjects at initial positions (range, DOA) of (5 m, -30°) and (5 m, $+30^\circ$), respectively, from the radar moving along straight paths away from the radar at a constant velocity of 1.3 m/s for a duration of 3 s as shown in Fig. 6a. The radar returns are simulated and processed via Eq. (7) to arrive at the Doppler–DOA distribution as a function of time. These time snapshots are summed in intensity to form a single plot of the Doppler–DOA tracks shown in Fig. 6b. It is observed that even though the Doppler returns of both the subjects are identical, it is possible to resolve the two subjects in the DOA domain. Note that both the Doppler and the DOA change slightly during the time duration. The Doppler spread that is observed in the figure is caused by the micro-Doppler components from the different body parts. In case 2, we consider two humans at initial positions (5 m, -30°) and (10 m, $+30^\circ$) from the radar as shown in Fig. 7a. The two subjects walk towards each other with a velocity of 1.3 m/s. Fig. 7b shows the Doppler–DOA tracks of the two humans. Since the

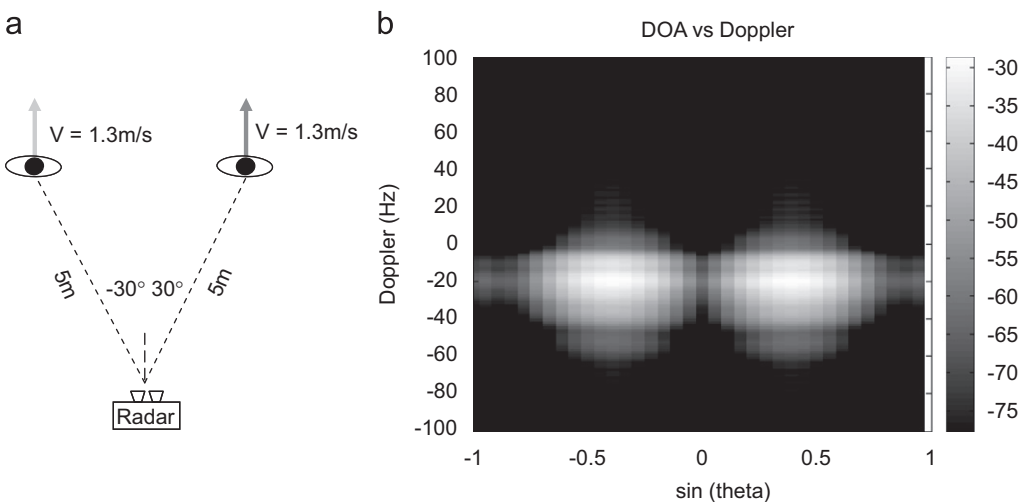


Fig. 6. (a) Case 1: Illustration of two human subjects’ motions. (b) Doppler–DOA tracks of the simulated radar returns of the two subjects.

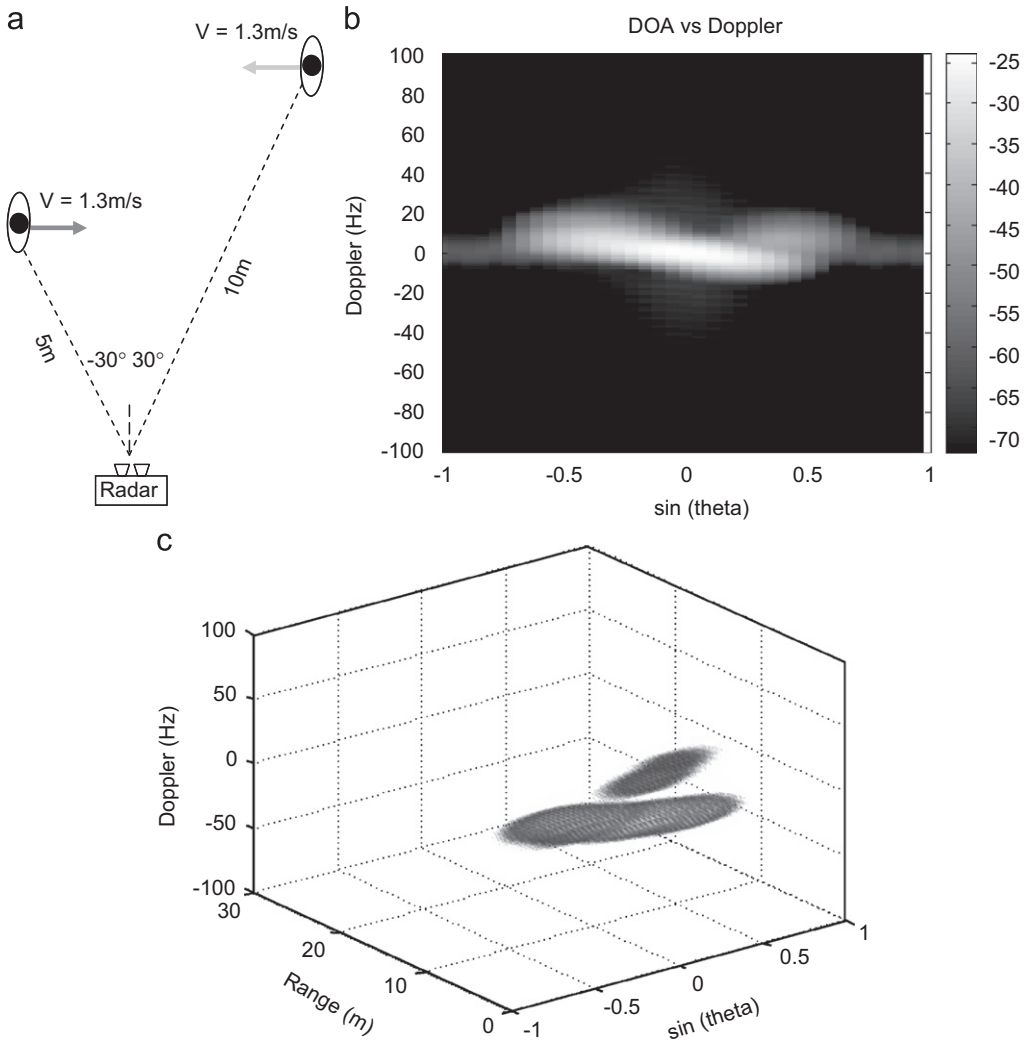


Fig. 7. (a) Case 2: Illustration of two human subjects' motions. (b) Doppler–DOA tracks of the simulated radar returns of the two subjects. (c) Doppler–DOA–Range tracks of the simulated radar returns of the two subjects.

subjects approach the radar at identical velocities, the Doppler returns are almost identical. The radial velocity is low and hence the micro-Doppler spread of the Doppler track is much weaker in this case. Initially the humans are well resolved in the DOA space. However, as they come closer, they are overlapped in the DOA domain and are no longer resolvable. Hence a higher order dimensionality is required for resolving the human movers in this case which is discussed in the next section.

4.3. Combining Doppler processing with spatial beamforming and ranging

To add ranging capability, we assume a stepped frequency waveform of bandwidth, β , and an antenna array of N elements. Let $x(f_c, n, t)$ be the downconverted time domain

radar returns of each element, n , for each carrier frequency f_c . It is assumed that the sweep time of the stepped frequency waveform is small so that the position and DOA of the human mover remain constant during the sweep. The three-dimensional transform of $x(f_c, n, t)$ based on Eq. (8) resolves the targets in the Doppler–DOA-range space:

$$X(r, \sin \theta_{AZ}, f, t') = \int_{f_c} \sum_n \int_t x(f_c, n, t) e^{-j2\pi f t} h(t' - t) dt e^{-j(n-1)(2\pi f_o d/c) \sin \theta_{AZ}} e^{+j2\pi f_c (2r/c)} df_c \quad (8)$$

In Eq. (8), the STFT operation transforms the time domain returns to the Doppler domain using the time window $h(t)$. Spatial beamforming is performed to resolve the targets along the DOA (θ_{AZ}) domain. A narrowband approximation (center frequency f_o) is used in this step to decouple the DOA from the range. This is followed by the inverse Fourier transform of the frequency (f_c) swept data to obtain the range, r .

Such processing is first tested on the simulated radar returns of human movers for case 2 that was described in Section 4.2. The time snapshots of the 3-D Doppler–DOA-range distribution of the returns have been summed in intensity and shown in a single plot in Fig. 7c. It is observed that, unlike Fig. 7b, the 3-D tracks of the two human movers do not intersect. Hence the two humans are well resolved during the entire time duration. The procedure is repeated for case 3, where the initial positions of the two movers are (5 m, -30°) and (10 m, -30°), respectively, and they walk away from the radar along a straight path at 1.3 m/s (see Fig. 8a). In this case there is overlap in both the Doppler and DOA domains. However, they are well resolved along the range domain as shown in Fig. 8b. Both the cases illustrate the advantages of incorporating a higher order dimensionality to the system. Of course this is accomplished at increased system cost and complexity.

4.4. Measured results

The concept of Doppler processing combined with spatial beamforming is next tested on measured data obtained from two human subjects walking in indoor line-of-sight environments. The measurements are made using a modified 2.4 GHz CW radar testbed described in Section 3. An antenna array consisting of four microstrip antenna elements is constructed. An inter-element spacing of $0.56 \lambda_c$ is used to avoid any grating lobes within the field of view of -45° to $+45^\circ$. Each antenna element is connected to a separate receiver channel.

The time domain radar returns from the multi-element array are processed using Eq. (7) to obtain the Doppler–DOA distribution as a function of time. However, since a limited size array is used, the beamforming technique is plagued with poor resolution and high sidelobes. In particular, the sidelobes of a strong target can overshadow a weaker target when they have overlapping Dopplers. One method of reducing the effect of high sidelobes is to use the CLEAN algorithm [28,36] after the spatial beamforming. In this algorithm, the strongest target is first identified as the peak in the beamforming pattern. Next, its main lobe and sidelobe features are subtracted from the pattern. This allows the weaker targets to be better revealed in the residual pattern and the process is repeated to extract the next strongest target. The algorithm is iterated until the energy in the residual pattern reaches a sufficiently low level. This algorithm is applied to every Doppler bin to obtain the Doppler–DOA distribution.

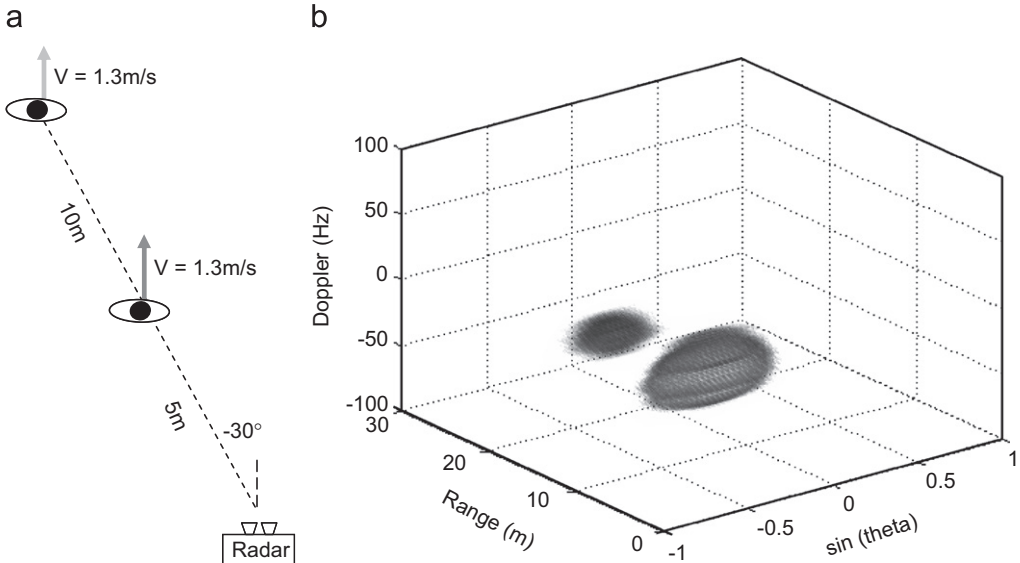


Fig. 8. (a) Case 3: Illustration of two human subjects' motions. (b) Doppler–DOA–Range tracks of the simulated radar returns of the two subjects.

In the measurement, subject 1 moves from the radar's right to its left. Subject 2 walks in the opposite direction to subject 1 as shown in Fig. 9a. Doppler processing and spatial beamforming in conjunction with CLEAN are applied to the radar returns. Fig. 9b shows the resulting Doppler–DOA distribution. Two distinct tracks that crisscross in the Doppler–DOA space are observed. At the start time, the Doppler returns from both subjects are positive. When they reach the radar boresight, their Doppler returns are both zero. At the end of the time period, both subjects have negative Doppler. Although there is considerable overlap in the Doppler domain, the DOA of the two movers are well resolved for most of the time duration. Results for multiple human movers in through-wall scenarios are discussed in [28].

5. Wall effects

One of the major challenges in the tracking of humans is the accuracy of the DOA measurements under through-wall operations. To better understand the wall propagation phenomenology, we present in this section some measurement and simulation results in connection with the operation of the Doppler-based radar testbed.

The two important wall effects on RF signal propagation are the attenuation of the signal amplitude through the wall and the phase distortion of the signal due to multipath and reverberation. For the signal attenuation, measurements are performed for different types of walls using the Doppler radar testbed at 2.4 GHz. An audio loudspeaker driven by a single tone is used as a calibration target. Measurements are carried out for line-of-sight (no wall), in situ with a gypsum/wooden wall in an interior room (see Fig. 10a), and in situ with an exterior brick wall (see Fig. 10b). The processed radar returns show a two-way path loss of 16 dB for the gypsum/wooden wall and 20 dB for the 15 in brick wall. Due to

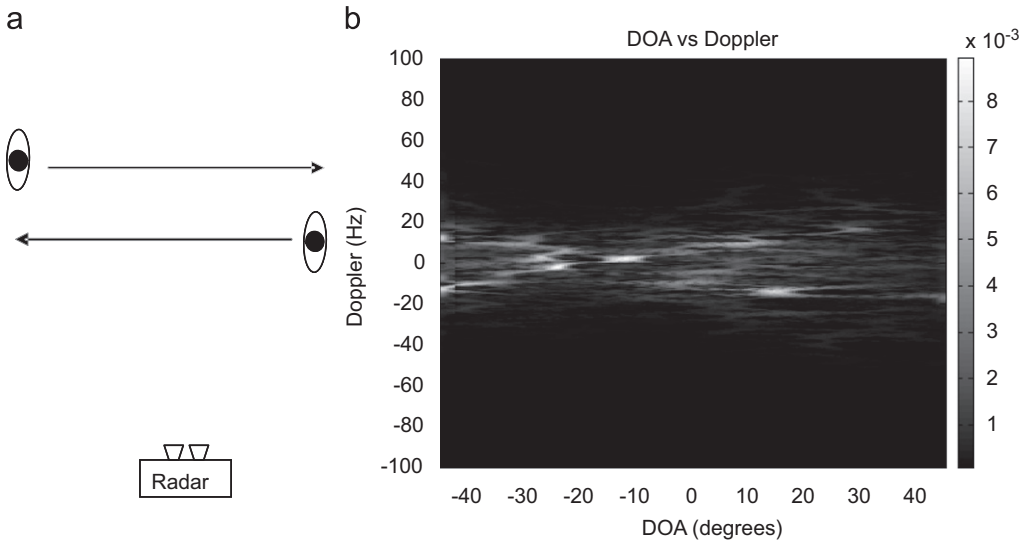


Fig. 9. (a) Illustration of two human subjects' motions. (b) Doppler–DOA tracks of the measured radar returns of the two subjects.



Fig. 10. (a) 5 in wooden/gypsum interior wall, (b) 15 in brick exterior wall, (c) 30 cm cinder block wall.

the significant attenuation of the signal through the wall, the signal-to-noise ratio of the system is considerably lowered. However, the more detrimental effect is the phase distortion introduced by the wall, as shown in the next series of measurements.

In order to study the effect of the wall on the received signal phase, a detailed measurement of target azimuth and elevation positions are made in indoor line-of-sight conditions using the three-element testbed discussed in Section 3. Here, a transmitting horn antenna is excited at $f_c(2.4\text{ GHz}) + \Delta f$ using a signal generator to simulate the Doppler

return of a moving target. The received signal is downconverted, digitized and processed by the radar in order to obtain the azimuth and elevation estimates of the horn positions. Fig. 11a shows the various measurement positions of the transmitting horn and Fig. 11b shows the corresponding two-dimensional DOA estimates. It is observed that the measured estimates agree very well with the actual positions of the horn. Next the measurements are repeated on a 6 ft cinder block wall that was constructed in our laboratory as shown in Fig. 10c. The wall is made of 30 cm thick cinder blocks stacked on top of each other. The measurements are repeated with the radar receiver at a distance of 30 cm from the wall. Fig. 11c show the two-dimensional DOA estimates obtained for the through-wall setup. In this case the transmitted signal travels only a one way path through the wall. It is seen that there is considerable error in the DOA estimation in spite of the strong received power level.

To help us understand the transmission physics, a two-dimensional FDTD simulation is carried out on both a solid homogeneous wall and a Cinder block wall structure with air holes. The thicknesses of both walls are 30 cm, with relative permittivity of the concrete set at 5. A 2.4 GHz sinusoidal source is used and the distance between the source and the wall is 30 cm in both cases. As can be seen in the sinusoidal steady-state field plots of Fig. 12a and b, the wavefront transmitted through the solid homogeneous wall remains a well behaved spherical front, while the transmitted wave through the inhomogeneous cinder block wall shows considerable reverberation near the wall. This complex wavefront leads to the poor DOA results observed in the measurement data. We also notice that at a sufficiently far distance from the wall, the wavefront begins to resemble the regular spherical spread. In essence, the cinder block structure acts like an array that re-radiates the impinging wavefront. Therefore, in the near field of the array, the transmitted field is quite complex. When sufficient distance is reached, the wavefront approaches that of the far field. The actual far-field distance depends on the illuminated aperture of the wall from the primary source.

Hence it may be possible to overcome the poor DOA estimation for an inhomogeneous wall by increasing the standoff distance of the radar from the wall. This is tried by performing a series of more precise phase measurements using a vector network analyzer

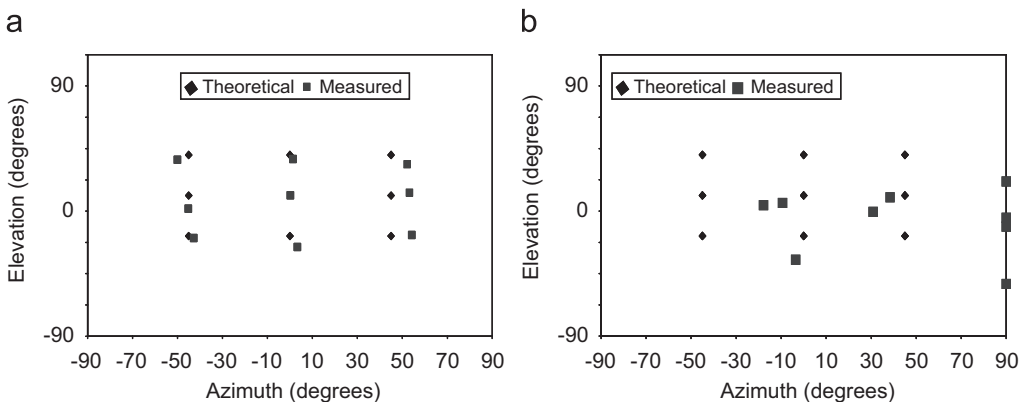


Fig. 11. DOA (azimuth and elevation) position measurements with three elements DDOA Radar in: (a) indoor LOS conditions and (b) through-wall conditions with Cinder block wall.

(VNA) under the tuned receiver mode. A two-element microstrip antenna array is connected to the two tuned receivers of the VNA and their measured phase difference is determined. A horn antenna is used as the transmitter and placed 3 ft in front of the cinder block wall as shown in Fig. 13a. The receiver is placed at different standoff distances (R) behind the wall as shown in Fig. 13b. At each distance, measurements are taken at three positions: at boresight (with respect to the transmitter), 3 ft to the right and 3 ft to the left of the boresight position. In each case, the azimuth DOA of the horn antenna is estimated by Eq. (4). Fig. 13c shows the azimuth DOA estimates for various positions of the receiver array. For reference, the truth values are also plotted as dashed lines. It is observed that when the receive array is very close to the wall, the DOA estimates are completely

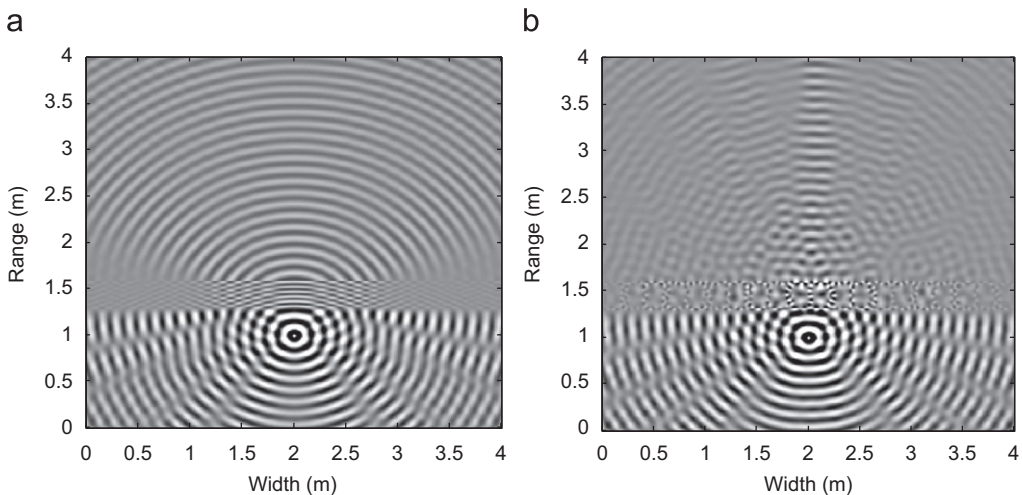


Fig. 12. FDTD results of wave propagation through: (a) a solid homogeneous wall and (b) an inhomogeneous cinder block wall.

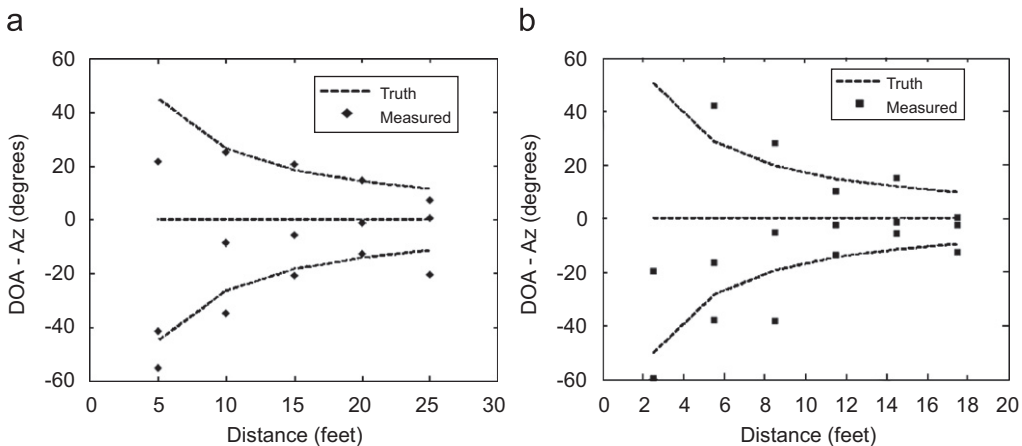


Fig. 13. VNA-based measurements of DOA (azimuth) of horn target, with a Receiver 2 element array for different stand off positions from: (a) cinder block wall and (b) exterior brick wall.

erroneous. The error in the estimates decreases as the standoff distance of the radar is increased beyond 10 ft. At the last position, the error again increases, most likely caused by the drop in the signal strength. The same measurements are also repeated for the exterior brick wall. The results are presented in Fig. 13d. Again, note that the DOA accuracy actually improves at sufficiently far distances away from the wall, provided that the signal strength is not too weak.

In summary, our study showed that a wall with interior inhomogeneity causes significant degradation to the transmitted wavefront, which leads to errors in the DOA estimates and hurts the tracking performance. Such distortion can be partially alleviated by allowing for a sufficient standoff distance between the radar and the wall. More fundamentally, the inhomogeneous wall effects need to be deconvolved from the desired target returns [37,38]. However, this requires more detailed knowledge of the thickness, the constituency of the wall and the wall dispersion effects [39].

6. Conclusion

In this paper, we have presented the principles of Doppler processing to detect and track human movers in indoor environments. The main advantage of Doppler sensing is that stationary clutters can be suppressed. The potential application of micro-Doppler features for the identification of human movements and the presence of carried objects was discussed. The RJTF was investigated as an alternate representation of the Doppler spectrogram that provides improved signal localization compared to the standard STFT. A three-dimensional (azimuth, elevation and range) radar concept that requires only three antenna elements and two frequency tones to track multiple movers was reviewed. This concept was based on using Doppler separation to discriminate the movers. However, the presence of micro-Doppler spread caused deterioration in the performance of the system. Additional dimensionality was then explored by using an antenna array for spatial beamforming, along with a multiple frequency waveform for range estimation. The performance improvement in multiple human tracking was illustrated using simulations and measurements. We also investigated the walls effects on Doppler-based detection and tracking. It was found that the phase distortion through a cinder block wall resulted in significant error in the accuracy of DOA estimation. It was also found that one way to partially alleviate this effect is to increase the standoff distance of the radar from the wall.

We conclude this paper by highlighting some areas that we believe warrant further research. First, the detection and tracking of humans through inhomogeneous walls remain a challenging problem. While Doppler processing allows the suppression of stationary clutters, the wall effect on Doppler shifted signals still needs to be properly characterized. Hence the study of through-wall phenomenology and methods to mitigate its effect remains one of the most important areas for future work. Second, the motion-induced imaging of human movers is potentially an interesting research topic. Traditional motion-induced imaging algorithms (such as the inverse synthetic aperture radar) have been derived for rigid body targets under regular rotational motions. However, human motion kinematics are quite complex, as can be seen from the human micro-Doppler data. Whether such motions can be exploited for imaging is still an open question. An attempt at the frontal imaging of a human by processing the micro-Doppler data from the different body parts was reported in [40]. However, research into more general approaches is still much needed. Finally, a simulation tool for studying radar signatures from human

motions will be an important capability for further developments in human detection, tracking and imaging. Sophisticated radar simulators have been developed for conventional air and ground targets. These simulators have proven to be indispensable in radar target recognition. A similar kind of radar simulator for humans under dynamic motions in indoor environments will provide us with the capability to pinpoint cause-and-effect and to generate training data for algorithm development. It can serve as an enabler to designing sensors with optimal performance.

Acknowledgments

This work was supported by the Office of Naval Research, the Texas Higher Education Coordinating Board under the Texas Advanced Technology Program, the National Science Foundation Major Research Instrumentation Program and NSF Grant CBET-0730924.

References

- [1] G. Franceschetti, J. Tatoi, D. Giri, G. Gibbs, Timed arrays and their application to impulse SAR for through-the-wall imaging, in: *IEEE Antennas and Propagation Society International Symposium Digest*, vol. 3, June 2004, pp. 3067–3070.
- [2] S. Nag, M.A. Barnes, T. Payment, G. Holladay, Ultrawideband through-wall radar for detecting the motion of people in real time, in: *SPIE Proceedings of the Radar Sensor Technology and Data Visualization*, vol. 4744, July 2002, pp. 48–57.
- [3] A.M. Attiya, A.M. Bayram, A. Safaai-Jazi, S.M. Raid, UWB applications for through wall detection, in: *IEEE Antennas and Propagation Society International Symposium Digest*, vol. 3, June 2004, pp. 3079–3082.
- [4] Y. Yang, A.E. Fathy, See-through-wall imaging using ultra-wideband short-pulse radar system, in: *IEEE Antennas and Propagation Society International Symposium Digest*, vol. 3B, July 2005, pp. 334–337.
- [5] A.R. Hunt, A wideband imaging radar for through-the-wall surveillance, in: *SPIE Proceedings of the Sensors, and Command, Control, Communications, and Intelligence (C3I) Technologies*, vol. 5403, September 2004, pp. 590–596.
- [6] F. Ahmad, G.J. Frazer, S.A. Kassam, M.G. Amin, Design and implementation of near field wideband synthetic aperture beamformer, *IEEE Trans. Aerosp. Electron. Systems* 40 (2004) 206–220.
- [7] L.M. Frazier, Radar surveillance through solid materials, in: *SPIE Proceedings of the Command, Control, Communications, and Intelligence Systems*, vol. 2938, February 1997, pp. 139–146.
- [8] T.B. Gibson, J.C. Jenn, Prediction and measurement of wall insertion loss, *IEEE Trans. Antennas Propagat.* 47 (1999) 55–57.
- [9] J.L. Geisheimer, E.F. Greneker, W.S. Marshall, High-resolution Doppler model of the human gait, in: *SPIE Proceedings of the Radar Sensor Technology and Data Visualization*, vol. 4744, July 2002, pp. 8–18.
- [10] V.C. Chen, H. Ling, *Time Frequency Transforms for Radar Imaging and Signal Analysis*, Artech House, Boston, MA, 2002.
- [11] P. van Dorp, F.C.A. Groen, Human walking estimation with radar, *IEE Proc. Radar Sonar Navig.* 150 (2003) 356–365.
- [12] M. Otero, Application of continuous wave radar for human gait recognition, in: *SPIE Proceedings of the Signal Processing, Sensor Fusion, and Target Recognition XIV*, vol. 5809, May 2005, pp. 538–548.
- [13] M.D. Anderson, R.L. Rogers, Micro-Doppler analysis of multiple frequency continuous wave radar signatures, in: *SPIE Proceedings of the Radar Sensor Technology XI*, vol. 6547, May 2007, p. 65470A.
- [14] L.M. Frazier, Surveillance through walls and other opaque materials, in: *Proceedings of the IEEE National Radar Conference Electronic Systems*, May 1996, pp. 27–31.
- [15] E.F. Greneker, Radar flashlight for through the wall detection of humans, in: *SPIE Proceedings of the Targets and Backgrounds: Characterization and Representation IV*, vol. 3375, April 1998, pp. 280–285.
- [16] E.F. Greneker, J.L. Geisheimer, D.S. Andreasen, O.D. Asbel, B.L. Stevens, B.S. Mitchell, Radar flashlight three years later: an update on developmental progress, in: *IEEE Annual International Carnahan Conference on Security Technology, Proceedings*, October 2000, pp. 257–259.

- [17] D.G. Falconer, R.W. Ficklin, K.W. Konelige, Robot mounted through wall radar for detecting, locating and identifying building occupants, in: Proceedings of the International Conference on Robotics and Automations, vol. 2, April 2000, pp. 1868–1878.
- [18] K. Kodera, C. De Villedary, R. Gendrin, Analysis of time varying signals with small BT values, *IEEE Trans. Acoust. Speech Signal Process.* 26 (1978) 64–76.
- [19] F. Auger, P. Flandrin, Improving the readability of time frequency and time scale representations by the reassignment method, *IEEE Trans. Signal Process.* 43 (1995) 1068–1089.
- [20] S.A. Fulop, K. Fitz, Algorithms for computing the time-corrected instantaneous frequency (reassigned) spectrogram, with applications, *J. Acoust. Soc. Am.* 119 (1) (2006) 360–371.
- [21] T.J. Gardner, M.O. Magnasco, Sparse time–frequency representations, *Proc. Natl. Acad. Sci.* 103 (16) (2006) 6094–6099.
- [22] A. Lin, H. Ling, Three-dimensional tracking of humans using a very low-complexity radar, *Electron. Lett.* 42 (2006) 1062–1064.
- [23] A. Lin, H. Ling, Human tracking using a two-element array, *SPIE Proc.* 5788 (2005) 57–64.
- [24] A. Lin, H. Ling, Through wall measurements of a Doppler and direction of arrival (DDOA) radar for tracking indoor movers, in: *IEEE Antennas and Propagation Society International Symposium Digest*, vol. 3B, July 2005, pp. 322–325.
- [25] A. Lin, H. Ling, A Doppler and direction-of-arrival (DDOA) radar for multiple-mover sensing based on a two-element array, to appear, *IEEE Trans. Aerosp. Electron. System* (2007).
- [26] A. Lin, H. Ling, Two-dimensional human tracking using a three-element Doppler and direction-of-arrival (DDOA) radar, in: *IEEE Radar Conference*, April 2006, pp. 248–251.
- [27] A. Lin, H. Ling, Location tracking of indoor movers using a two-frequency Doppler and direction-of-arrival (DDOA) radar, in: *IEEE Antennas and Propagation Society International Symposium Digest*, July 2006, pp. 1125–1128.
- [28] S.S. Ram, Y. Yang, A. Lin, H. Ling, Human tracking using Doppler processing and spatial beamforming, in: *IEEE Radar Conference*, April 2007, pp. 546–551.
- [29] T. Thayaparan, S. Abrol, E. Riseborough, L. Stankovic, D. Lamothe, G. Duff, Analysis of radar micro-Doppler signatures from experimental helicopter and human data, *IEE Proc. Radar Sonar Navig.* 1 (4) (2007) 288–299.
- [30] T. Thayaparan, L. Stanković, I. Djurović, Micro-Doppler human signature detection and its application to gait recognition and indoor imaging, *J. Franklin Inst.* (2008) (Special Issue on Indoor Radar Imaging).
- [31] R. Bouluc, M.N. Thalmann, D. Thalmann, A global human walking model with real-time kinematic personification, *Vis. Comput.* 6 (1990) 344–358.
- [32] M.G. Anderson, Multiple frequency continuous wave radar for microDoppler extraction, Master's Thesis, University of Texas at Austin, May 2005.
- [33] F. Ahmad, M.G. Amin, P. Setlur, Through-the-wall target localization using dual-frequency CW radars, in: *SPIE Proceedings of the Symposium on Defense and Security, Sensors, and Command, Control, Communications, and Intelligence (C3I) Technologies Conference*, vol. 6201, Orlando, FL, April 2006.
- [34] M. Amin, P. Zeman, P. Setlur, F. Ahmad, Moving target localization for indoor imaging using dual frequency CW radars, in: *Proceedings of the Fourth IEEE Workshop on Sensor Array and Multi-Channel Processing (SAM2006)*, Waltham, MA, July 2006, pp. 367–371.
- [35] F. Ahmad, M.G. Amin, P.D. Zeman, Performance analysis of dual-frequency CW radars for motion detection and ranging in urban sensing applications, in: *SPIE Proceedings of the Symposium on Defense and Security, Radar Sensor Technology XI Conference*, vol. 6547, Orlando, FL, April 2007.
- [36] J. Tsao, B.D. Steinberg, Reduction of sidelobe and speckle artifacts in microwave engineering: the CLEAN technique, *IEEE Trans. Antennas Propagat.* 36 (1988) 543–556.
- [37] M. Dehmollaian, K. Sarabandi, Refocusing through building walls using synthetic aperture radar, in: *IEEE Antennas and Propagation Society International Symposium Digest*, June 2007, pp. 1465–1468.
- [38] P.B. Weichman, Ultra-fast forward modeling of microwave propagation through multipathing media for efficient solution of tomographic inverse problems, *URSI National Radio Science Meeting Digest*, July 2007.
- [39] A. Muqaibel, et al., Characterization of wall dispersive and attenuative effects on UWB radar signals, *J. Franklin Inst.* (2008) (Special Issue on Indoor Radar Imaging).
- [40] A. Lin, H. Ling, Frontal imaging of humans using three element Doppler and direction of arrival radar, *Electron. Lett.* 42 (11) (2006) 660–661.